Parabrachial CGRP Neurons Establish and Sustain Aversive Taste Memories

Highlights

- Parabrachial CGRP neurons are critical for conditioned taste aversion (CTA) learning

- After CTA learning, parabrachial CGRP neurons exhibit synaptic plasticity

- Parabrachial CGRP neurons are re-activated during expression of CTA

- Silencing or inhibiting CGRP neurons prevents expression of CTA

Authors

Jane Y. Chen, Carlos A. Campos,
Brooke C. Jarvie, Richard D. Palmiter

Correspondence

palmiter@uw.edu

In Brief

Conditioned taste aversion (CTA) develops when ingestion of a novel food is accompanied by gastrointestinal malaise. Chen et al. demonstrate that parabrachial CGRP neurons are not only necessary for learning CTA but are also active during expression of those memories.

Neuron

Article

Parabrachial CGRP Neurons Establish and Sustain Aversive Taste Memories

Jane Y. Chen,[1,2,3] Carlos A. Campos,[1,2] Brooke C. Jarvie,[1,2,3] and Richard D. Palmiter[1,2,4,*]
[1]Howard Hughes Medical Institute, University of Washington, Seattle, WA 98195, USA
[2]Departments of Biochemistry and Genome Sciences, University of Washington, Seattle, WA 98195, USA
[3]Graduate Program in Neuroscience, University of Washington, Seattle, WA 98195, USA
[4]Lead Contact
*Correspondence: palmiter@uw.edu
https://doi.org/10.1016/j.neuron.2018.09.032

SUMMARY

Food aversions develop when the taste of a novel food is associated with sickness, which often occurs after food poisoning or chemotherapy treatment. We identified calcitonin-gene-related peptide (CGRP) neurons in the parabrachial nucleus (PBN) as sufficient and necessary for establishing a conditioned taste aversion (CTA). Photoactivating projections from CGRP[PBN] neurons to either the central nucleus of the amygdala or the bed nucleus of the stria terminalis can also induce robust CTA. CGRP[PBN] neurons undergo plasticity following CTA, and inactivation of either *Arc* or *Grin1* (genes involved in memory consolidation) prevents establishment of a strong CTA. Calcium imaging reveals that the novel food re-activates CGRP[PBN] neurons after conditioning. Inhibition of these neurons or inactivation of the *Grin1* gene after conditioning attenuates CTA expression. Our results indicate that CGRP[PBN] neurons not only play a key role for learning food aversions but also contribute to the maintenance and expression of those memories.

INTRODUCTION

Animals have innate preferences for tastes accompanying calorically rich foods and aversions to tastes associated with potentially spoiled or toxic foods. In addition, they possess learning mechanisms to modify feeding behavior based on their experience. If ingestion of a food is followed by gastrointestinal malaise, animals avoid consuming that food in the future. This phenomenon, known as conditioned taste aversion (CTA), protects animals against repeated consumption of toxic food. Taste aversion learning is considered a type of classical Pavlovian conditioning, where an association is formed between the food (conditioned stimulus [CS]) and subsequent malaise (unconditioned stimulus [US]). To develop a strong CTA, both the food and the malaise must be novel. A remarkable feature of CTA is that the ingestion of food and subsequent visceral malaise can be separated by hours, suggesting that an engram (or

memory) of the novel food persists long after initial exposure (Reilly, 2009).

Despite its importance as a critical survival mechanism, the neural integration of taste and malaise signals underlying the food memory is poorly understood. Ascending gustatory and visceral signals follow parallel but distinct paths from the cranial nerves to the nucleus of the solitary tract and then the parabrachial nucleus (PBN). From the PBN, taste information is relayed through the gustatory thalamus (parvicellular part of ventral posteriomedial thalamus [VPMpc]) and gustatory cortex (Spector, 2009). Nociceptive visceral signals are relayed through the PBN to the central nucleus of the amygdala (CeA), bed nucleus of the stria terminalis (BNST), thalamus, and hypothalamus (Lundy and Norgren, 2015). Although separate pathways relay gustatory and visceral signals, interconnectivity between many of these regions (Reilly and Bornovalova, 2005; Yamamoto and Ueji, 2011) complicate efforts to identify where the association between taste and illness occurs to produce an aversive taste memory.

A seminal study, which observed that decerebrate rats failed to acquire a CTA (Grill and Norgren, 1978), sparked the search for forebrain regions responsible for taste aversion learning. Lesions of many forebrain regions impair CTA acquisition, though none completely abolish CTA learning (Reilly, 2009). However, lesions of the PBN disrupt the transmission of ascending US signals and consequently prevent learning the association between CS and US (Reilly, 1999; Spector et al., 1992).

In the laboratory, CTA is commonly modeled by pairing a novel food or taste with exposure to lithium chloride (LiCl), lipopolysaccharide (LPS), or other compounds that induce nausea and malaise (Garcia et al., 1955; Ingram, 1982). Systemic administration of LiCl or LPS induces Fos, a marker of neuronal activity, in the PBN, which co-localizes in part to neurons that express the calcitonin-gene-related peptide (CGRP) (Carter et al., 2013). Stimulating CGRP[PBN] neurons is sufficient to induce a CTA, and inhibition of these neurons attenuates LiCl-induced CTA (Carter et al., 2015). However, it is unclear whether inhibition of CGRP[PBN] neurons prevents the acquisition or the expression of the memory. After CTA acquisition, the taste induces Fos in the external lateral PBN, where CGRP neurons reside (Swank and Bernstein, 1994; Tokita et al., 2007). Furthermore, CGRP[PBN] neurons can also respond to a cue after fear conditioning (Campos et al., 2018). Therefore, we hypothesized that activation of CGRP[PBN] neurons may also be necessary for the expression
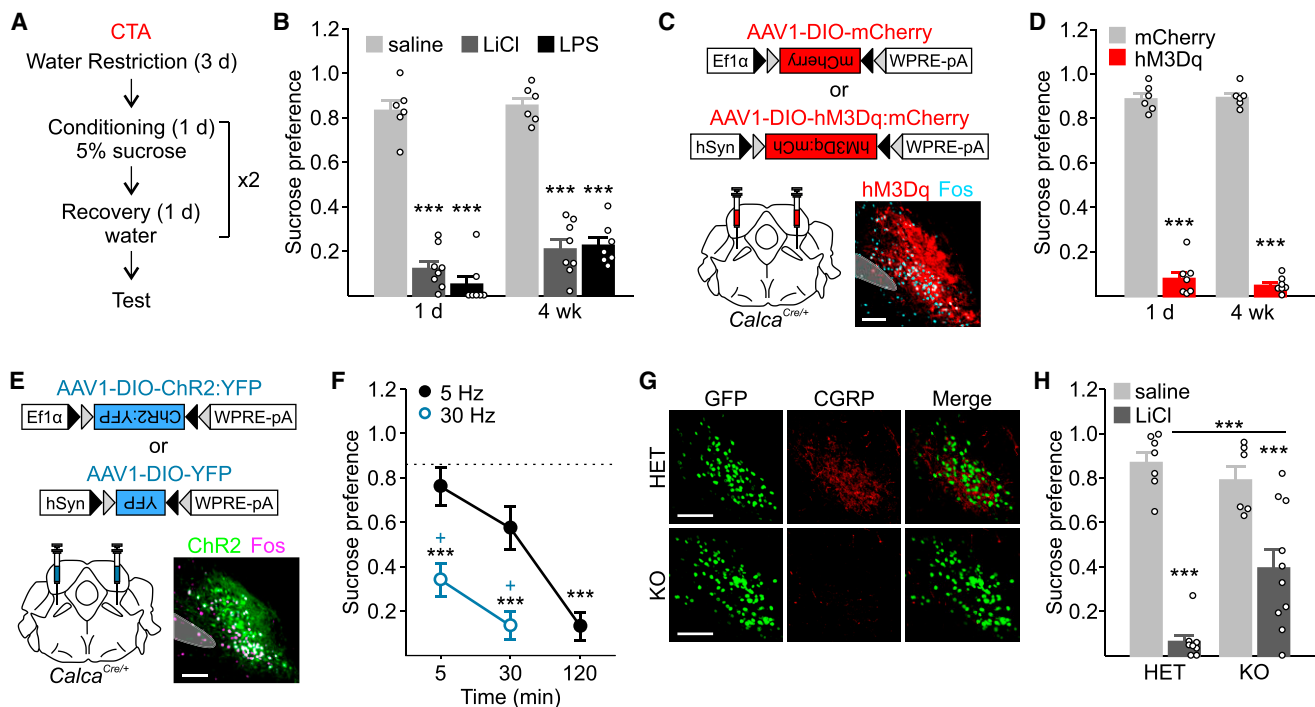
Figure 1. Activation of CGRP^PBN Neurons Induces CTA and Involves Release of CGRP

(A) CTA conditioning timeline.

(B) Pairing LiCl or LPS with novel sucrose induces CTA that persists for 4 weeks (n = 6 saline, n = 8 LiCl, n = 7 LPS; two-way repeated measures [RM] ANOVA; treatment: $F_{2,18}$ = 173.78; p < 0.001).

(C) Bilateral injections of AAV1-DIO-hM3Dq:mCherry or AAV1-DIO-mCherry into the PBN of $Calca^{Cre/+}$ mice with representative image of viral expression and induction of Fos in the PBN after CNO administration. Scale bar, 100 μm.

(D) Pairing CNO activation of CGRP^PBN neurons with exposure to 5% sucrose causes a robust and long-lasting CTA (n = 6 mCherry, n = 7 hM3Dq; two-way RM ANOVA; treatment: $F_{1,5}$ = 405.84, p < 0.001).

(E) Bilateral injections of AAV1-DIO-ChR2:YFP or AAV1-DIO-YFP and fiber optic cannula implants into the PBN of $Calca^{Cre/+}$ mice. Representative image shows viral expression and induction of Fos in the PBN after photostimulation. Scale bars, 100 μm.

(F) Robust CTA is acquired with low-frequency, long-duration optogenetic stimulation or high-frequency, short-duration stimulation of CGRP^PBN neurons (n = 5 for each group; one-way ANOVA; interaction $F_{5,20}$ = 18.847; p < 0.001). Dashed line represents mice injected with YFP and stimulated at 5 or 30 Hz (sucrose preference, 0.86 ± 0.09). Significant differences between groups compared to YFP are denoted by *, and significance between 5 and 30 Hz at 5 or 30 min is denoted by +.

(G) Cre:GFP (green) and CGRP expression (red) in $Calca^{Cre/+}$ (HET) and $Calca^{Cre/Cre}$ (KO) mice. Scale bar, 100 μm.

(H) CGRP KO mice have attenuated LiCl-induced CTA (HET: n = 7 saline, n = 8 LiCl; KO: n = 6 saline, n = 10 LiCl; two-way ANOVA; interaction $F_{1,27}$ = 8.86; p = 0.006).

Data are reported as mean ± SEM. ***p < 0.001.

of a CTA. We delivered viruses expressing Cre-dependent genes into the brain of mice with Cre-recombinase targeted to the $Calca$ locus, which encodes CGRP, to selectively manipulate the activity or gene expression of CGRP^PBN neurons to investigate their roles in acquiring and expressing a CTA.

RESULTS

Activation of CGRP^PBN Neurons Induces CTA and Involves Release of CGRP

We developed a paradigm to induce a robust and persistent CTA by acclimating mice to a restricted drinking schedule in cages with two water bottles for 3 days. On day 4, water was replaced with access to a novel taste (5% sucrose) for 30 min followed by an injection of saline, LiCl (180 mg/kg), or LPS (50 μg/kg). Mice were given water access the next day then

the conditioning paradigm was repeated. CTA was measured on day 8 with a two-bottle preference test comparing sucrose intake to total fluid intake (water + sucrose) during a 30-min period (preference = sucrose/total fluid consumption; Figure 1A). LiCl- or LPS-injected animals developed a robust CTA (sucrose preference < 0.2) that persisted for at least 4 weeks after conditioning (Figure 1B).

Because LiCl and LPS both activate CGRP^PBN neurons, we asked whether artificial activation of these neurons can induce a robust and persistent CTA. Mice were bilaterally injected with an adeno-associated virus carrying an excitatory receptor in a Cre-dependent manner (AAV1-DIO-hM3Dq:mCherry), which is exclusively activated by clozapine-N-oxide (CNO), into the PBN of $Calca^{Cre/+}$ mice. Pairing sucrose with an injection of CNO (1 mg/kg) resulted in a robust and long-lasting CTA (Figures 1C and 1D), similar to LiCl- or LPS-induced CTA.

LiCl, LPS, and CNO activation of CGRP neurons all have long-lasting effects that persist for >2 hr (Carter et al., 2013), but a brief 5-min stimulation of CGRP neurons is also sufficient to induce CTA (Carter et al., 2015). To determine the optimal stimulation parameters for CTA, we used optogenetics with channelrhodopsin, a light-activated cation channel, tagged with a yellow fluorescent protein (YFP) to vary the stimulus frequency and duration of activation of CGRP^{PBN} neurons. We bilaterally injected AAV1-DIO-ChR2:YFP and implanted fiber optic cannulas over the PBN (Figure 1E). Pairing 5% sucrose with low-frequency, long-duration photostimulation (5 Hz for 120 min) or high-frequency, short-duration stimulation (30 Hz for 30 min) was sufficient to induce a robust CTA, whereas low-frequency, short-duration stimulation (5 Hz for 5 min or 30 min) did not result in CTA (Figure 1F).

To examine the role of CGRP signaling in CTA, we used homozygous $Calca^{Cre/Cre}$ mice; the Cre:GFP cassette includes a polyadenylation signal inserted into the 2nd exon, which precludes expression of the downstream exon encoding CGRP. Immunohistochemistry staining for CGRP in the PBN of $Calca^{Cre/Cre}$ mice confirmed the absence of CGRP-positive fibers in these knockout (KO) mice (Figure 1G). Pairing novel sucrose with an injection of LiCl in CGRP KO mice attenuated development of CTA compared to heterozygous (HET) controls (Figure 1H). Interestingly, chemogenetic activation of CGRP^{PBN} neurons expressing hM3Dq in CGRP KO mice still produced a strong CTA (sucrose preference: 0.049 ± 0.00875 in HET and 0.159 ± 0.0942 in KO mice; n = 5–6 mice per group; Mann-Whitney rank sum test; $U = 9$; p = 0.180). Thus, LiCl-induced CTA requires release of CGRP, but direct activation of CGRP^{PBN} neurons can induce CTA independently of CGRP release.

CGRP^{PBN} Neurons Undergo Plasticity after CTA

As CTA involves learning, we asked whether CGRP^{PBN} neurons undergo plasticity after conditioning. We measured the ratio of α-amino-3-hydroxy-5-methyl-4-isoxazolepropionic acid (AMPA) to N-methyl-D-aspartate (NMDA) receptor currents and frequency of spontaneous excitatory post-synaptic currents (sEPSCs) after CTA. To enhance visualization of CGRP neurons, AAV1-DIO-mCherry was injected into the PBN of $Calca^{Cre/+}$ mice, which co-localized with endogenous Cre:GFP expression (Figures 2A and 2B). Mice were conditioned with 5% sucrose and LiCl injection (as in Figure 1A) and tested for acquisition of CTA 2 days after the last conditioning trial. LiCl-injected (CTA) mice showed a significant increase in AMPA/NMDA ratio compared to control saline-injected mice (Figures 2C and 2D). The increase in AMPA/NMDA ratio was accompanied by a significant increase in the frequency, but not amplitude, of sEPSCs recorded from CTA mice (Figures 2E–2G).

We also examined the role of Arc, an immediate early gene implicated in memory consolidation (Plath et al., 2006), and $Grin1$, which encodes the essential NR1 subunit of the NMDA receptor and is involved in Arc induction, in the development of CTA. To knock out Arc or $Grin1$ selectively in CGRP^{PBN} neurons, we generated a conditional mouse, in which Cre expression at the $Calca$ locus is dependent on FLP recombinase ($Calca^{frtCre/+}$; Figure S1). These mice were bred to mice with conditional Arc or $Grin 1$ alleles (Figures S2A–S2C) to generate $Calca^{frtCre/+}::Arc^{lox/lox}$ or $Calca^{frtCre/+}::Grin1^{lox/lox}$ (KO) mice. Littermates with

the genotype $Calca^{frtCre/+}::Grin1^{lox/+}$ or $Calca^{frtCre/+}::Arc^{lox/+}$ (HET) were used as controls. Injection of AAV1-FLP:DsRed and AAV1-DIO-YFP into the PBN allowed expression of Cre and Cre-dependent YFP in CGRP^{PBN} neurons (Figure 2H), which then inactivated the Arc or $Grin1$ gene in those cells to produce cell-specific KO. Non-CGRP neurons express FLP:DsRed, but not Cre-dependent YFP (Figure 2H, inset). Expression of Cre resulted in the absence of Arc expression in $Arc^{lox/lox}$ mice (unpublished data) and abolished NMDAR-mediated currents in $Grin1^{lox/lox}$ mice (Figure S3A).

If either Arc or $Grin1$ was knocked out in CGRP^{PBN} neurons prior to conditioning, mice were unable to acquire a CTA (Figures 2I–2K). Inactivation of Arc after CTA was acquired had no effect on the established memory (Figures 2L and 2M). However, if $Grin1$ was inactivated after conditioning, the previously learned aversion was attenuated (Figure 2N).

As NMDA receptor (NMDAR) KO may produce changes in excitability, we recorded the firing rate of $Grin1$ KO neurons in response to current injection and found that $Grin1$ KO neurons were less excitable than controls (Figures S3B and S3C). However, an injection of LiCl decreased food intake in both $Calca^{frtCre/+}::Grin1$ HET and KO mice (Figure 2O), suggesting that the decrease in excitability does not affect the normal physiological response to LiCl. Together, these results indicate that $Grin1$ contributes to both the acquisition and expression of CTA, whereas Arc is necessary for acquisition, but not retention or expression, of CTA.

CGRP^{PBN} Neurons Are Active during Expression of CTA

CGRP^{PBN} neuron activation can act as the US during CTA learning, and these neurons undergo synaptic plasticity after CTA. Therefore, we hypothesized that the novel taste (CS) could act as an US after conditioning by re-activating CGRP^{PBN} neurons. To test this hypothesis, mice were injected with AAV1-DIO-GCaMP6m, a fluorescent calcium indicator, and implanted with a gradient-index lens over the PBN to monitor CGRP neuronal activity in awake animals (Figure 3A). After a single conditioning trial with 30-min access to a novel food (vanilla Ensure), mice were given an injection of LPS (50 μg/kg) or saline for controls. Two days later, mice were videotaped during re-exposure to Ensure while changes in fluorescence were recorded with miniature microscope (Inscopix) that allows visualization of calcium activity in individual CGRP-expressing neurons. We observed little change in fluorescence of CGRP^{PBN} neurons when Ensure was not present. In mice that received LPS (CTA), fluorescence increased in virtually all of the neurons after Ensure was presented, which was not observed in control mice that received saline (Figures 3B and 3D). Although some changes in fluorescence coincided with head movements (Video S1; Figures S4A and S4B), there was no significant correlation between movement distance and changes in fluorescence after Ensure was presented (Figures 3C, S4A, and S4B). In contrast, when control mice approached the Ensure bottle, there was relatively little change in CGRP-neuron fluorescence (Figures 3B and 3D; Video S2). The average locomotor activity of CTA mice was less than control mice during re-exposure to Ensure (Figure 3E). Under anesthesia, presentation of a cotton swab dipped in Ensure increased fluorescence of CGRP neurons of CTA mice,
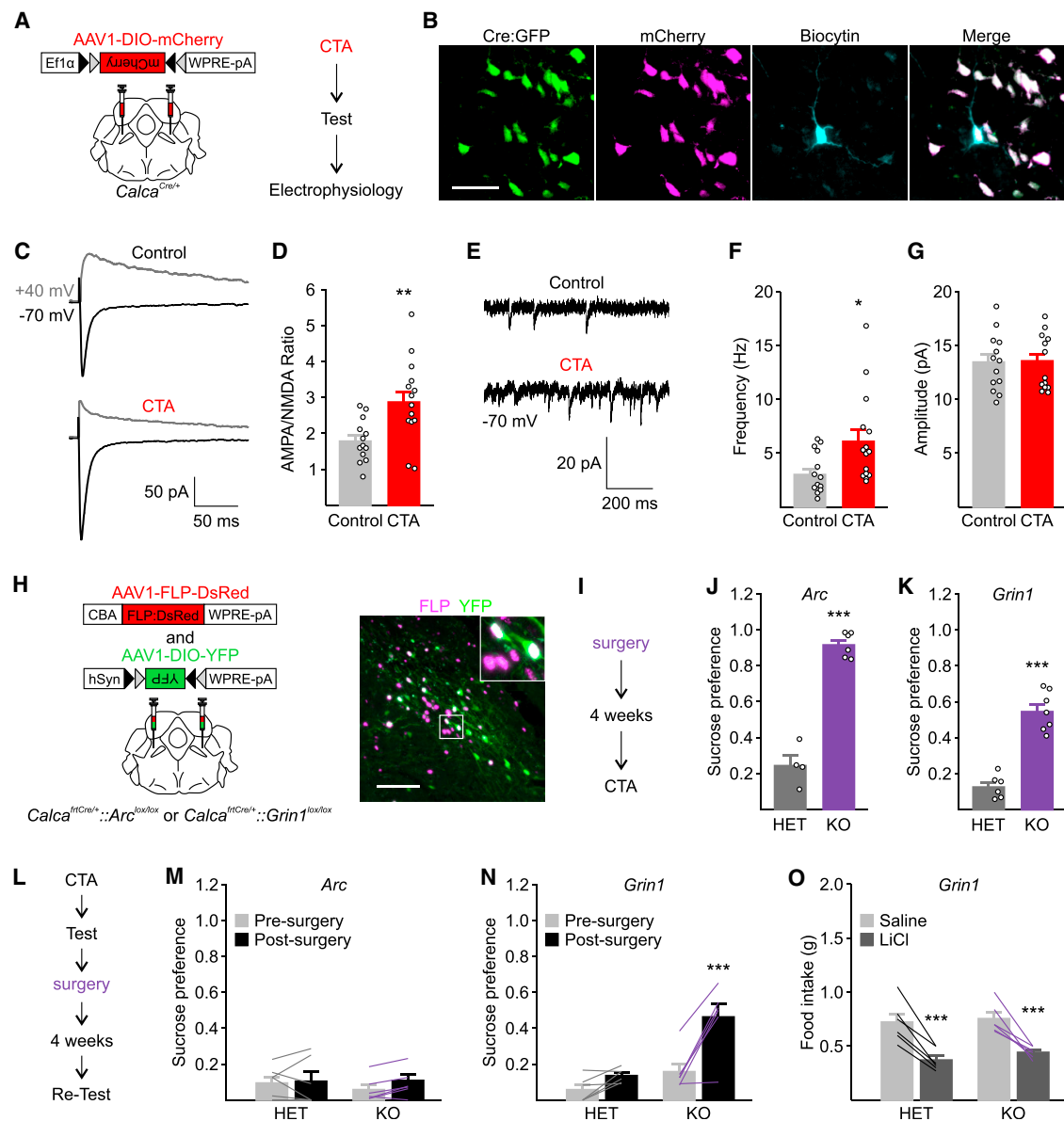
Figure 2. CGRP^PBN Neurons Undergo Plasticity after CTA

(A) Bilateral injection of AAV1-DIO-mCherry into PBN of $Calca^{Cre/+}$ mice.

(B) Representative image of CGRP neuron co-expressing GFP and mCherry filled with biocytin during recording. Scale bar, 50 μm.

(C) Representative traces of AMPAR- and NMDAR-mediated currents recorded from CGRP neurons of control (top) and CTA (bottom) mice.

(D) Ratios of peak AMPAR- to NMDAR-mediated currents (control: n = 13 cells from 4 mice; CTA: n = 15 cells from 4 mice; unpaired two-tailed Student's t test; $t(26) = -3.153$; p = 0.004).

(E) Representative traces of sEPSCs from control (top) and CTA (bottom) mice.

(F) Average frequency of sEPSCs (control: n = 14 cells from 4 mice; CTA: n = 15 cells from 4 mice; Mann-Whitney rank sum test; $U = 50$; p = 0.017).

(G) Average amplitude of sEPSCs (control: n = 14 cells from 4 mice; CTA: n = 15 cells from 4 mice; unpaired two-tailed Student's t test; $t(27) = -0.112$; p = 0.912).

(H) Bilateral injection of AAV1-FLP:DsRed and AAV1-DIO-YFP into PBN of $Calca^{frtCre/+}::Grin1^{lox/lox}$ or $Calca^{frtCre/+}::Arc^{lox/lox}$ mice results in FLP:DsRed and Cre-dependent YFP expression in the PBN. Scale bar, 100 μm.

(I) Experimental timeline for inactivation of Arc or $Grin1$ prior to CTA.

(J and K) Inactivation of Arc (J) or $Grin1$ (K) in CGRP^PBN neurons prior to conditioning attenuates LiCl-induced CTA (Arc: n = 4 HET, n = 6 KO, unpaired two-tailed Student's t test, $t(8) = -11.701$, p < 0.001; $Grin1$: n = 6 HET, n = 7 KO, Mann-Whitney rank sum test, $U = 0$, p = 0.001).

(L) Experimental timeline for inactivation of Arc or $Grin1$ after CTA.

(M and N) Inactivating $Grin1$ (N), but not Arc (M), after conditioning blocks expression of CTA (n = 6 for each group; $Grin1$: two-way RM ANOVA, interactions: $F_{1,10} = 10.677$, p = 0.008; Arc: two-way RM ANOVA, interaction: $F_{1,10} = 1.142$, p = 0.310).

(O) Inactivation of $Grin1$ does not affect LiCl-induced reduction of food intake (n = 6 in each group; two-way RM ANOVA; treatment: $F_{1,10} = 69.781$; p < 0.001). Data are reported as mean ± SEM. *p < 0.05; **p < 0.01; ***p ≤ 0.001. See also Figures S1, S2, and S3.
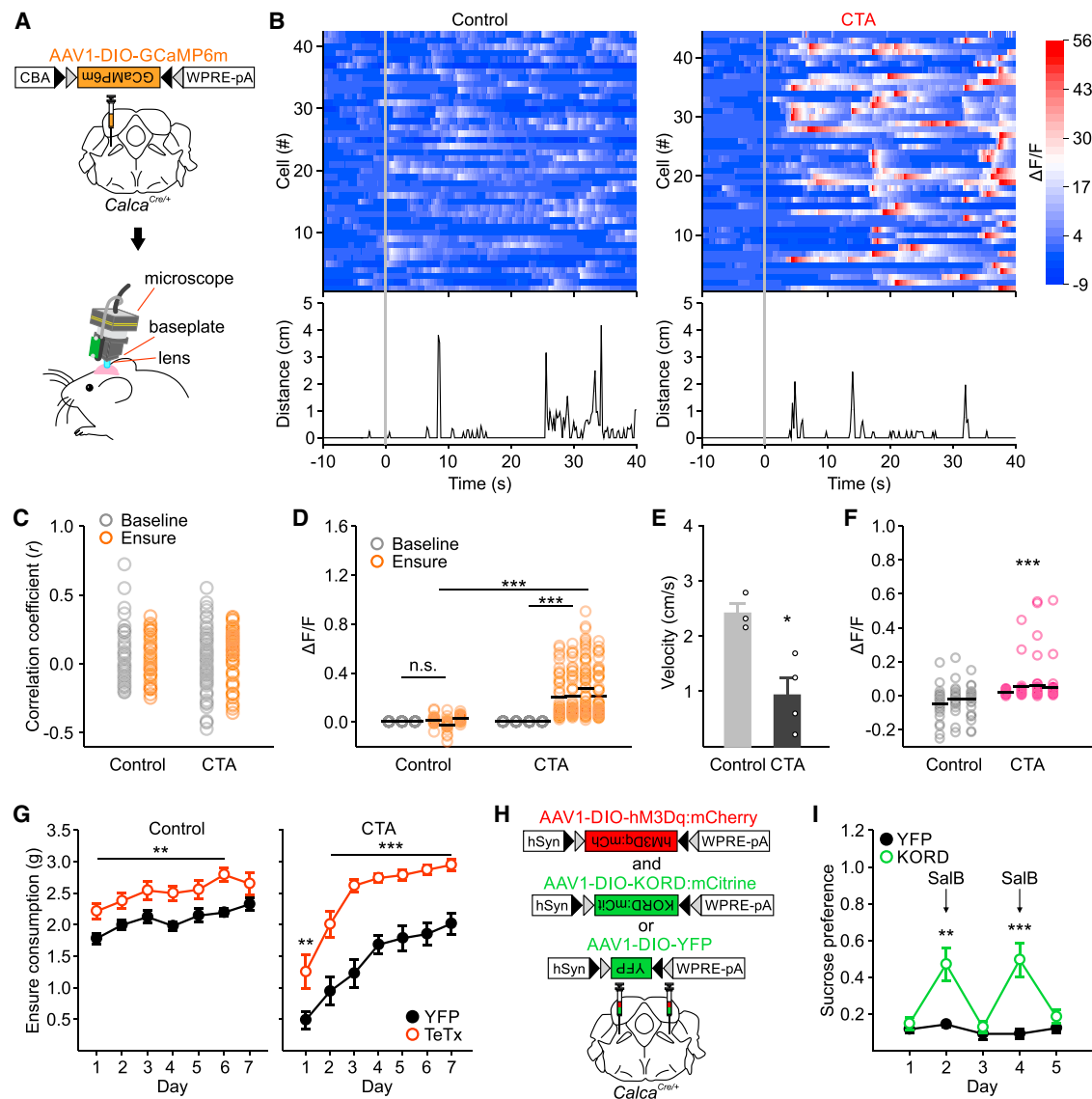
Figure 3. CGRP^{PBN} Neurons Are Active during Expression of CTA

(A) Injection of AAV1-DIO-GCaMP6m into the PBN of *Calca$^{Cre/+}$* mice and diagram of calcium imaging setup.

(B) Sample responses of CGRP^{PBN} neurons before and after Ensure presentation (top) and corresponding head movements (bottom) of a control (left) and CTA-treated (right) mouse.

(C) Correlation coefficients for the changes in fluorescence of each cell and head movements of mice shown in (B). There was no significant change in correlation coefficients after Ensure was presented (two-way RM ANOVA; time: $F_{1,104} = 2.100$; p = 0.343).

(D) Responses of CGRP^{PBN} neurons at baseline (30 s) and after Ensure presentation (90 s). Each column represents all cells recorded from the same mouse (control: n = 134 neurons from 3 mice; CTA: n = 202 neurons from 4 mice). The average population response from each mouse, indicated by the horizontal black line, was used for statistical analysis (two-way RM ANOVA; interaction $F_{1,5} = 83.358$; p < 0.001).

(E) Average movement velocity of control and CTA mice during re-exposure to Ensure (control: 3 mice; CTA: 4 mice; unpaired two-tailed Student's t test; t(5) = 3.538; p = 0.017). *p < 0.05.

(F) Responses of CGRP^{PBN} neurons to the smell of Ensure while mice are under anesthesia. Each column represents all cells recorded from the same mouse (control: n = 134 neurons from 3 mice; CTA: n = 202 neurons from 4 mice). The average population response from each mouse, indicated by the horizontal black line, was used for statistical analysis (unpaired two-tailed Student's t test; t(5) = −6.299; p = 0.001).

(G) Pairing Ensure with injection of LPS results in a strong CTA; pairing novel Ensure with saline does not induce CTA (left), whereas inactivation of CGRP neurons with TeTx after learning attenuates CTA (left) during 7 days of extinction testing (n = 10 in each group; two-way RM ANOVA; virus: $F_{1,108} = 32.217$; p < 0.001). In agreement with previous findings (Campos et al., 2016), TeTx-treated mice consume more Ensure than YFP controls (n = 6 in each group; two-way RM ANOVA; virus: $F_{1,60} = 11.554$; p = 0.007).
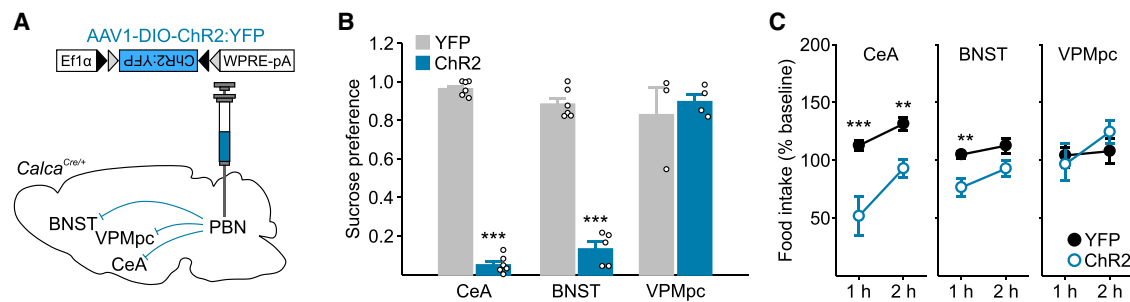
(legend continued on next page)

Figure 4. Stimulation of CGRP[PBN] Projections Induces CTA

(A) Bilateral injections of AAV1-DIO-ChR2:YFP or AAV1-DIO-YFP into the PBN of $Calca^{Cre/+}$ mice with fiber optic cannula implants into the CeA, BNST, or VPMpc.

(B) Pairing stimulation of CGRP[PBN] projections (30 min at 30 Hz) to the CeA or BNST, but not the VPMpc, with novel sucrose induces CTA (B; CeA: n = 5 YFP, n = 6 ChR2, unpaired two-tailed Student's t test, $t(10) = 37.504$, $p < 0.001$; BNST: n = 6 YFP, n = 5 ChR2, unpaired two-tailed Student's t test, $t(9) = 15.484$, $p < 0.001$; VPMpc: n = 3 YFP, n = 4 ChR2, unpaired two-tailed Student's t test, $t(5) = -0.519$, $p = 0.626$).

(C) Photostimulation of axonal projections to CeA and BNST, but not VPMpc, reversibly inhibits food intake (CeA: n = 5 YFP, n = 6 ChR2, two-way RM ANOVA, virus: $F_{1,8} = 15.142$, $p = 0.005$; BNST: n = 6 YFP, n = 5 ChR2, two-way RM ANOVA, virus: $F_{1,8} = 9.489$, $p = 0.015$; VPMpc: n = 8 YFP, n = 8 ChR2, two-way RM ANOVA, virus: $F_{1,28} = 0.908$, $p = 0.357$).

Data are reported as mean ± SEM. **$p < 0.01$; ***$p < 0.001$. See also Figure S6.

but not control mice (Figure 3F), demonstrating that CGRP neurons can be activated by the smell of Ensure in the absence of locomotion. These results reveal that the CS (taste and/or smell of Ensure) can act as an US after conditioning.

To explore the functional role of CGRP[PBN] neurons in the expression of CTA, we silenced CGRP[PBN] neurons with tetanus toxin (AAV1-DIO-GFP:TeTx) after establishing a CTA. These mice consumed more Ensure during 7 days of extinction compared to control mice (Figure 3G). Silencing CGRP[PBN] neurons increased Ensure intake in control mice, so we also examined the effects of transiently inhibiting CGRP[PBN] neurons during CTA expression. $Calca^{Cre/+}$ mice were co-injected with AAV1-DIO-hM3Dq:mCherry and AAV1-DIO-KORD:mCitrine (an inhibitory receptor activated by salvinorin B [SalB]) to bidirectionally modulate CGRP neural activity (Figure 3H). Pairing 5% sucrose with activation of CGRP[PBN] neurons via CNO induced a strong CTA, but inhibition of the neurons with SalB prior to testing attenuated expression of CTA, and this pattern was repeated with subsequent testing (Figure 3I). When CNO and SalB were co-administered, the suppression of food intake caused by activation of CGRP[PBN] neurons was also attenuated (Figure S5A). In agreement, co-injection of CNO and SalB reduced the number of Fos-positive cells observed in the PBN (Figures S5B and S5C), indicating that SalB effectively inhibits neurons that otherwise would be activated by CNO. These results support the observation that not only are CGRP[PBN] neurons activated by the CS after learning, but their activity is important for expression of a previously learned CTA.

Stimulation of CGRP[PBN] Projections Results in CTA

Because CGRP[PBN] neurons send strong projections to the CeA, BNST, and VPMpc (Figure S6), we investigated the effects of

stimulating each of these downstream sites on CTA by injecting AAV1-DIO-ChR2:YFP into the PBN and placing bilateral fiber optic cannulas over each of the target regions (Figure 4A). Pairing stimulation of CGRP[PBN] projections to the CeA or BNST (30 Hz for 30 min) with 5% sucrose induced CTA and reduced food intake for 1 or 2 hr (Figures 4B and 4C), whereas stimulating the projection to the VPMpc had no effect. These data suggest that there is redundant circuitry involved in CTA learning.

DISCUSSION

We demonstrated that pairing a novel food with either LiCl or LPS is sufficient to generate a robust and long-lasting CTA in which CGRP itself plays a role. Direct chemogenetic or optogenetic activation of CGRP[PBN] neurons without peripheral visceral malaise is also sufficient to induce CTA. Importantly, we also reveal that CGRP[PBN] neurons undergo plasticity after learning and that their activity is necessary for expression of CTA. *Grin1* expression within CGRP[PBN] neurons is necessary for acquisition and expression of CTA, and *Arc* is only necessary for CTA acquisition. Stimulation of CGRP[PBN] projections to either the CeA or BNST mimics CTA induced by stimulation of CGRP[PBN] cell bodies. Although we suspect that mice develop a conditioned aversion to sucrose or Ensure, our assay only measures consumption; thus, our experiments do not distinguish between taste aversion and avoidance (Dwyer et al., 2017; Garcia and Koelling, 1966).

We observed that CGRP KO mice develop an attenuated CTA, which supports the idea that LiCl activation of CGRP[PBN] neurons stimulates release of CGRP to facilitate learning the taste aversion. In agreement, pairing saccharin with an intracerebroventricular administration of CGRP results in a mild CTA (Krahn

(H) Bilateral injection of AAV1-DIO-hM3Dq:mCherry and AAV1-DIO-KORD:mCitrine or AAV1-DIO-YFP into PBN of $Calca^{Cre/+}$ mice for bidirectional modulation of CGRP[PBN] neuron activity.

(I) Pairing CNO activation of CGRP[PBN] neurons with novel sucrose induces CTA, and subsequent inhibition of the same neurons with SalB on days 2 and 4 of testing prevents expression of CTA (n = 7 YFP; n = 16 KORD; two-way RM ANOVA; interaction: $F_{1,84} = 7.787$; $p < 0.001$).

Data are reported as mean ± SEM. **$p < 0.01$; ***$p \leq 0.001$. See also Figures S4 and S5 and Videos S1 and S2.

CellPress

et al., 1986), indicating that CGRP can participate in development of a CTA. CGRP neurons are glutamatergic (Carter et al., 2013), and they express several other neuropeptides, including β-CGRP (unpublished observations), suggesting that CGRP may be one of several signaling molecules that are involved in generating a CTA. In contrast to LiCl-mediated CTA, development of CTA after chemogenetic activation of CGRP[PBN] neurons was unaffected by loss of CGRP. A likely explanation for this disparity is that direct chemogenetic activation of CGRP[PBN] neurons is more robust than that achieved by LiCl; hence, release of the other transmitters makes CGRP unnecessary.

Learning to avoid a potentially toxic taste ultimately requires consolidation of a long-term memory. Our finding that CGRP[PBN] neurons exhibit synaptic plasticity after learning suggests that the PBN is involved in not only CTA acquisition but also the expression of the learned aversion. Inactivation of *Arc*, an immediate early gene involved in memory consolidation (Plath et al., 2006), prevents establishment of CTA. This indicates a critical role for synaptic plasticity in these neurons during formation of an aversive taste memory. As induction of *Arc* requires NMDA receptor activation (Chen et al., 2017; Steward and Worley, 2001), knocking out NMDA receptors (*Grin1* KO) in CGRP[PBN] neurons also prevents establishment of a CTA. Interestingly, inactivation of *Grin1* in these neurons after learning attenuated expression of CTA, suggesting that the CS activation of CGRP[PBN] neurons after learning also requires signaling through NMDA receptors. Furthermore, because *Arc* is only involved in memory consolidation (Nakayama et al., 2015; Ploski et al., 2008), not expression, it follows that inactivation of *Arc* in CGRP[PBN] neurons after learning has no effect on CTA expression.

We demonstrated that, after conditioning, the CS can re-activate CGRP[PBN] neurons. Transiently inhibiting (KORD with SalB) or permanently silencing (TeTx) these neurons after learning attenuated the expression of a CTA and promoted extinction. Previously, we showed that activation of CGRP[PBN] neurons reduces food intake (Carter et al., 2013) and is aversive (Han et al., 2015), which indicates that they relay the US during conditioning. Following the traditional model of Pavlovian conditioning, after an association between the CS and US is formed, the CS acts similar to the US to elicit behavioral responses (Fanselow and Wassum, 2015; Rescorla, 1988). However, the neurocircuitry that allows the CS to mimic the US signal has not been identified. Most models suggest that synaptic plasticity within target neurons where the CS and US signals converge allows the CS to activate the US-responsive neurons (Johansen et al., 2011; Maren, 2005; Sah et al., 2008). These experiments provide evidence that, after conditioning, the CS activates the CGRP[PBN] neurons, which initially relayed the US signal. In agreement, CGRP[PBN] neurons also respond to the CS after fear conditioning (Campos et al., 2018). The neural circuitry that allows the CS to activate US-responsive neurons after learning remains to be elucidated.

Taken together, these data reveal a critical role of CGRP[PBN] neurons in both the acquisition and expression of an aversive taste memory. Furthermore, the frequency and duration of CGRP[PBN] stimulation influences the strength of the CTA acquired. Consequently, either severe malaise lasting for a short period or weak malaise lasting for an extended time can promote a strong CTA. That latter situation is commonly observed with food poisoning and chemotherapy.

The downstream neurons that mediate this learning have yet to be identified. Our observation that stimulation of CGRP[PBN] projections to either the CeA or BNST can result in CTA indicates that there may be redundant circuitry involved in CTA learning. In agreement, previous studies have shown that lesions of the CeA or BNST have no effect on learning a CTA (Morris et al., 1999; Reilly and Bornovalova, 2005; Roman et al., 2006; Yamamoto et al., 1995). This may be due to the reciprocal connections within the CeA and BNST (Douglass et al., 2017; Gungor et al., 2015; Yu et al., 2017), as well as their nearly identical inputs and target projections (Haufler et al., 2013; Lebow and Chen, 2016). Although many studies have focused on the amygdala as a point of convergence between the taste and visceral malaise signals (Reilly and Bornovalova, 2005), our data suggest that this CS-US association may form in multiple sites to give rise to a CTA.

STAR★METHODS

Detailed methods are provided in the online version of this paper and include the following:

- KEY RESOURCES TABLE
- CONTACT FOR REAGENT AND RESOURCE SHARING
- EXPERIMENTAL MODEL AND SUBJECT DETAILS
- METHOD DETAILS
  - Design of Calca-FLP-Dependent Cre Recombinase
  - Generation of Conditional Arc Mice
  - Virus Production
  - Stereotaxic Surgery
  - Photostimulation
  - Conditioned Taste Aversion (CTA) Assay
  - Measuring Food Intake
  - Calcium Imaging
  - Slice Electrophysiology
  - Pharmacological Injections
  - Histology and Microscopy
- QUANTIFICATION AND STATISTICAL ANALYSIS

SUPPLEMENTAL INFORMATION

Supplemental Information includes six figures and two videos and can be found with this article online at https://doi.org/10.1016/j.neuron.2018.09.032.

AUTHOR CONTRIBUTIONS

DECLARATION OF INTERESTS

REFERENCES

Campos, C.A., Bowen, A.J., Schwartz, M.W., and Palmiter, R.D. (2016). Parabrachial CGRP neurons control meal termination. Cell Metab. 23, 811–820.

Campos, C.A., Bowen, A.J., Roman, C.W., and Palmiter, R.D. (2018). Encoding of danger by parabrachial CGRP neurons. Nature 555, 617–622.

Carter, M.E., Soden, M.E., Zweifel, L.S., and Palmiter, R.D. (2013). Genetic identification of a neural circuit that suppresses appetite. Nature 503, 111–114.

Carter, M.E., Han, S., and Palmiter, R.D. (2015). Parabrachial calcitonin gene-related peptide neurons mediate conditioned taste aversion. J. Neurosci. 35, 4582–4586.

Chen, T., Zhu, J., Yang, L.K., Feng, Y., Lin, W., and Wang, Y.H. (2017). Glutamate-induced rapid induction of Arc/Arg3.1 requires NMDA receptor-mediated phosphorylation of ERK and CREB. Neurosci. Lett. 661, 23–28.

Douglass, A.M., Kucukdereli, H., Ponserre, M., Markovic, M., Gründemann, J., Strobel, C., Alcala Morales, P.L., Conzelmann, K.K., Lüthi, A., and Klein, R. (2017). Central amygdala circuits modulate food consumption through a positive-valence mechanism. Nat. Neurosci. 20, 1384–1394.

Dwyer, D.M., Gasalla, P., Bura, S., and López, M. (2017). Flavors paired with internal pain or with nausea elicit divergent types of hedonic responses. Behav. Neurosci. 131, 235–248.

Fanselow, M.S., and Wassum, K.M. (2015). The origins and organization of vertebrate pavlovian conditioning. Cold Spring Harb. Perspect. Biol. 8, a021717.

Garcia, J., and Koelling, R.A. (1966). Relation of cue to consequence in avoidance learning. Psychon. Sci. 4, 123–124.

Garcia, J., Kimeldorf, D.J., and Koelling, R.A. (1955). Conditioned aversion to saccharin resulting from exposure to gamma radiation. Science 122, 157–158.

Grill, H.J., and Norgren, R. (1978). Chronically decerebrate rats demonstrate satiation but not bait shyness. Science 201, 267–269.

Gungor, N.Z., Yamamoto, R., and Paré, D. (2015). Optogenetic study of the projections from the bed nucleus of the stria terminalis to the central amygdala. J. Neurophysiol. 114, 2903–2911.

Han, S., Soleiman, M.T., Soden, M.E., Zweifel, L.S., and Palmiter, R.D. (2015). Elucidating an affective pain circuit that creates a threat memory. Cell 162, 363–374.

Haufler, D., Nagy, F.Z., and Pare, D. (2013). Neuronal correlates of fear conditioning in the bed nucleus of the stria terminalis. Learn. Mem. 20, 633–641.

Ingram, D.K. (1982). Lithium chloride-induced taste aversion in C57BL/6J and DBA/2J mice. J. Gen. Psychol. 106 (2d Half), 233–249.

Johansen, J.P., Cain, C.K., Ostroff, L.E., and LeDoux, J.E. (2011). Molecular mechanisms of fear learning and memory. Cell 147, 509–524.

Krahn, D.D., Gosnell, B.A., Levine, A.S., and Morley, J.E. (1986). The effect of calcitonin gene-related peptide on food intake involves aversive mechanisms. Pharmacol. Biochem. Behav. 24, 5–7.

Krashes, M.J., Koda, S., Ye, C., Rogan, S.C., Adams, A.C., Cusher, D.S., Maratos-Flier, E., Roth, B.L., and Lowell, B.B. (2011). Rapid, reversible activation of AgRP neurons drives feeding behavior in mice. J. Clin. Invest. 121, 1424–1428.

Lebow, M.A., and Chen, A. (2016). Overshadowed by the amygdala: the bed nucleus of the stria terminalis emerges as key to psychiatric disorders. Mol. Psychiatry 21, 450–463.

Lundy, R.F., and Norgren, R. (2015). Gustatory System (Academic Press), pp. 891–921.

Maren, S. (2005). Synaptic mechanisms of associative memory in the amygdala. Neuron 47, 783–786.

Mattis, J., Tye, K.M., Ferenczi, E.A., Ramakrishnan, C., O'Shea, D.J., Prakash, R., Gunaydin, L.A., Hyun, M., Fenno, L.E., Gradinaru, V., et al. (2011). Principles for applying optogenetic tools derived from direct comparative analysis of microbial opsins. Nat. Methods 9, 159–172.

Morris, R., Frey, S., Kasambira, T., and Petrides, M. (1999). Ibotenic acid lesions of the basolateral, but not the central, amygdala interfere with conditioned taste aversion: evidence from a combined behavioral and anatomical tract-tracing investigation. Behav. Neurosci. 113, 291–302.

Nakayama, D., Iwata, H., Teshirogi, C., Ikegaya, Y., Matsuki, N., and Nomura, H. (2015). Long-delayed expression of the immediate early gene Arc/Arg3.1 refines neuronal circuits to perpetuate fear memory. J. Neurosci. 35, 819–830.

Plath, N., Ohana, O., Dammermann, B., Errington, M.L., Schmitz, D., Gross, C., Mao, X., Engelsberg, A., Mahlke, C., Welzl, H., et al. (2006). Arc/Arg3.1 is essential for the consolidation of synaptic plasticity and memories. Neuron 52, 437–444.

Ploski, J.E., Pierre, V.J., Smucny, J., Park, K., Monsey, M.S., Overeem, K.A., and Schafe, G.E. (2008). The activity-regulated cytoskeletal-associated protein (Arc/Arg3.1) is required for memory consolidation of pavlovian fear conditioning in the lateral amygdala. J. Neurosci. 28, 12383–12395.

Reilly, S. (1999). The parabrachial nucleus and conditioned taste aversion. Brain Res. Bull. 48, 239–254.

Reilly, S. (2009). Central Gustatory System Lesions and Conditioned Taste Aversion (Oxford University Press), pp. 309–327.

Reilly, S., and Bornovalova, M.A. (2005). Conditioned taste aversion and amygdala lesions in the rat: a critical review. Neurosci. Biobehav. Rev. 29, 1067–1088.

Rescorla, R.A. (1988). Pavlovian conditioning. It's not what you think it is. Am. Psychol. 43, 151–160.

Resendez, S.L., Jennings, J.H., Ung, R.L., Namboodiri, V.M., Zhou, Z.C., Otis, J.M., Nomura, H., McHenry, J.A., Kosyk, O., and Stuber, G.D. (2016). Visualization of cortical, subcortical and deep brain neural circuit dynamics during naturalistic mammalian behavior with head-mounted microscopes and chronically implanted lenses. Nat. Protoc. 11, 566–597.

Roman, C., Nebieridze, N., Sastre, A., and Reilly, S. (2006). Effects of lesions of the bed nucleus of the stria terminalis, lateral hypothalamus, or insular cortex on conditioned taste aversion and conditioned odor aversion. Behav. Neurosci. 120, 1257–1267.

Roman, C.W., Derkach, V.A., and Palmiter, R.D. (2016). Genetically and functionally defined NTS to PBN brain circuits mediating anorexia. Nat. Commun. 7, 11905.

Sah, P., Westbrook, R.F., and Lüthi, A. (2008). Fear conditioning and long-term potentiation in the amygdala: what really is the connection? Ann. N Y Acad. Sci. 1129, 88–95.

Sanford, C.A., Soden, M.E., Baird, M.A., Miller, S.M., Schulkin, J., Palmiter, R.D., Clark, M., and Zweifel, L.S. (2017). A central amygdala CRF circuit facilitates learning about weak threats. Neuron 93, 164–178.

Spector, A.C. (2009). Central Gustatory System and Ingestive Behavior (Academic Press), pp. 685–689.

Spector, A.C., Norgren, R., and Grill, H.J. (1992). Parabrachial gustatory lesions impair taste aversion learning in rats. Behav. Neurosci. 106, 147–161.

Steward, O., and Worley, P.F. (2001). Selective targeting of newly synthesized Arc mRNA to active synapses requires NMDA receptor activation. Neuron 30, 227–240.

CellPress

Swank, M.W., and Bernstein, I.L. (1994). c-Fos induction in response to a conditioned stimulus after single trial taste aversion learning. Brain Res. *636*, 202–208.

Tokita, K., Shimura, T., Nakamura, S., Inoue, T., and Yamamoto, T. (2007). Involvement of forebrain in parabrachial neuronal activation induced by aversively conditioned taste stimuli in the rat. Brain Res. *1141*, 188–196.

Tsien, J.Z., Huerta, P.T., and Tonegawa, S. (1996). The essential role of hippocampal CA1 NMDA receptor-dependent synaptic plasticity in spatial memory. Cell *87*, 1327–1338.

Vardy, E., Robinson, J.E., Li, C., Olsen, R.H.J., DiBerto, J.F., Giguere, P.M., Sassano, F.M., Huang, X.P., Zhu, H., Urban, D.J., et al. (2015). A new DREADD facilitates the multiplexed chemogenetic interrogation of behavior. Neuron *86*, 936–946.

Yamamoto, T., and Ueji, K. (2011). Brain mechanisms of flavor learning. Front. Syst. Neurosci. *5*, 76.

Yamamoto, T., Fujimoto, Y., Shimura, T., and Sakai, N. (1995). Conditioned taste aversion in rats with excitotoxic brain lesions. Neurosci. Res. *22*, 31–49.

Yu, K., Ahrens, S., Zhang, X., Schiff, H., Ramakrishnan, C., Fenno, L., Deisseroth, K., Zhao, F., Luo, M.H., Gong, L., et al. (2017). The central amygdala controls learning in the lateral amygdala. Nat. Neurosci. *20*, 1680–1685.

Zhou, P., Resendez, S.L., Rodriguez-Romaguera, J., Jimenez, J.C., Neufeld, S.Q., Giovannucci, A., Friedrich, J., Pnevmatikakis, E.A., Stuber, G.D., Hen, R., et al. (2018). Efficient and accurate extraction of in vivo calcium signals from microendoscopic video data. eLife *7*, e28728.

CellPress

STAR★METHODS

KEY RESOURCES TABLE

REAGENT or RESOURCE	SOURCE	IDENTIFIER
Antibodies		
Rabbit polyclonal anti-c-Fos	Abcam	ab190289
Goat polyclonal anti-c-Fos	Santa Cruz Biotechnology	Cat# sc-52, RRID: AB_2629503
Chicken polyclonal anti-GFP	Abcam	Cat# ab13970, RRID: AB_300798
Mouse monoclonal anti-CGRP	Abcam	Cat# ab81887, RRID: AB_1658411
Streptavidin, marina blue conjugate	Thermo Fisher Scientific	S11221
Alexa Fluor 488 donkey anti-chicken	Jackson ImmunoResearch	Cat# 703-545-155, RRID: AB_2340375
Alexa Fluor 594 donkey anti-mouse	Jackson ImmunoResearch	Cat# 715-585-150, RRID: AB_2340854
Cy5 donkey anti-goat	Jackson ImmunoResearch	Cat# 705-175-147, RRID: AB_2340415
Cy5 donkey anti-rabbit	Jackson ImmunoResearch	Cat# 711-175-152, RRID: AB_2340607
Normal donkey serum	Jackson ImmunoResearch	Cat# 017-000-121, RRID: AB_2337258
Bacterial and Virus Strains		
pAAV1-hSyn-DIO-hM3(Gq)-mCherry	Krashes et al., 2011	Addgene Plasmid #44361
pAAV1-Ef1α-DIO-mCherry	Bryan Roth, Carter et al., 2013	Addgene Plasmid #50462
pAAV1-Ef1α-DIO hChR2(E123A)-EYFP	Mattis et al., 2011	Addgene Plasmid #35507
pAAV1-hSyn-DIO-YFP	Karl Deisseroth, Carter et al., 2015	Similar to Addgene Plasmid #27056
pAAV1-Ef1α-DIO-synaptophysin-mCherry	Roman et al., 2016	N/A
pAAV1-CBA-Flippase-DsRed	Larry Zweifel, this paper	N/A
pAAV1-CBA-DIO-GCaMp6m	Larry Zweifel Sanford et al., 2017	N/A
pAAV1-hSyn-dF-HA-KORD-IRES-mCitrine	Vardy et al., 2015	Addgene Plasmid #65417
pAAV1-CBA-DIO-GFP:TeTx	Han et al., 2015	N/A
Chemicals, Peptides, and Recombinant Proteins		
Lithium chloride	Fisher Scientific	Cat# L121, CAS 7447-41-8
Lipopolysaccharide, *S. typhimurium*	Calbiochem	Cat# 437650
Clozapine-N-oxide	RTI	Cat# C929
Salvinorin B	Cayman Chemical	Cat# 11488, CAS 92545-30-7
Bicuculline methochloride	Tocris	Cat# 0131, CAS 53552-05-9
Biocytin	Sigma Aldrich	Cat# B4261, CAS 576-19-2
Experimental Models: Organisms/Strains		
Mouse: *Calca*^{Cre}	Carter et al., 2013	N/A
Mouse: *Calca*^{frtCre}	This paper	N/A
Mouse: *Arc*$^{lox/lox}$	This paper	N/A
Mouse: B6.129S4-*Grin1*^{tm2Stl}/J	The Jackson Laboratory	RRID: IMSR_JAX: 005246
Software and Algorithms		
SigmaPlot 12.0	Systat	https://systatsoftware.com/products/sigmaplot; RRID: SCR_010285
CorelDraw x6	Corel	https://www.coreldraw.com/en/; RRID: SCR_014235
pClamp10.3	Molecular Devices	https://www.moleculardevices.com/products/axon-patch-clamp-system/acquisition-and-analysis-software/pclamp-software-suite; RRID: SCR_011323
MiniAnalysis	Synaptosoft	http://www.synaptosoft.com/MiniAnalysis/; RRID: SCR_002184

Continued

REAGENT or RESOURCE	SOURCE	IDENTIFIER
MATLAB	MathWorks	https://www.mathworks.com/products/matlab.html; RRID: SCR_001622
Ethovision XT 10	Noldus Technology	https://www.noldus.com/; RRID: SCR_000441
Mosaic	Inscopix	https://www.inscopix.com
CNMF-E	GitHub	https://github.com/zhoupc/CNMF_E

CONTACT FOR REAGENT AND RESOURCE SHARING

Information and requests for resources and reagents should be directed to and will be fulfilled by the Lead Contact, Richard D. Palmiter (palmiter@uw.edu).

EXPERIMENTAL MODEL AND SUBJECT DETAILS

All experiments were approved by the University of Washington Institutional Animal Care and Use Committee and were performed in accordance with the guidelines described in the US National Institutes of Health Guide for the Care and Use of Laboratory Animals. All mice were backcrossed for >6 generations onto a C57BL/6 background. $Calca^{Cre/Cre}$, $Calca^{Cre/+}$, and $Grin1^{lox/lox}$ mice were generated as described previously (Carter et al., 2013, Tsien et al., 1996). $Calca^{frtCre/frtCre}::Grin1^{lox/lox}$ males were bred with $Grin1^{lox/+}$ females and $Calca^{frtCre/frtCre}::Arc^{lox/lox}$ males were bred with $Arc^{lox/+}$ females to generate KO and HET control mice. Knockout and control mice were identified by PCR of tail DNA. Both male and female mice were used for all experiments, aged 7-9 weeks at the start of experimental procedures and no more than 20 weeks at the end of experimental procedures. Mice were housed on a 12-h light/dark cycle (lights on 05:00-17:00) at ∼22°C with food and water available *ad libitum*, except during CTA and foodintake studies described below. Animals from the same litter were split randomly between control and experimental groups, with an equal number of male and female mice in each group.

METHOD DETAILS

Design of Calca-FLP-Dependent Cre Recombinase
A FLP-dependent Cre recombinase was constructed by inserting a *Mt1* gene intron within the open reading frame of mnCre:GFP, which has a Myc tag (m), followed by a nuclear localization signal (NLS, n), followed by Cre recombinase fused to green fluorescent protein (Cre:GFP), to generate a gene with two exons. Then the second exon was inverted and flanked by a pair of dissimilar frt sites to make a DIO construct. The action of FLP recombinase inverts the second exon allowing splicing to generate functional Cre recombinase. This cassette was substituted for Cre:GFP in the $Calca^{Cre:GFP}$ construct described previously (Carter et al., 2013) to generate $Calca^{frtCre}$ targeting construct (Figure S1). Mice with this construct were generated as described (Carter et al., 2013).

Generation of Conditional Arc Mice
To make the targeting construct, the 5′ arm (∼7.5 kb with *Pac*1 and *Sal*1 sites at each end) and the 3′ arm (∼5 kb with *Pme*1 and *Not*1 sites) were PCR amplified with Q5 DNA polymerase from a mouse C57BL/6 BAC clone. These arms were cloned into the polylinkers of targeting vector that includes a loxP site, frt-flanked Sv-Neo gene for positive selection and *Pgk*-DTa and HSV-TK genes for negative selection. A loxP site was inserted into the *BssH*1 site in the *Arc* promoter region; the other loxP site is in the first intron downstream of the first exon, which includes entire coding region (Figures S2A–S2C). Thus, Cre-mediated recombination removes the entire coding region. This construct was electroporated into G4 ES cells (C57BL/6 × 129/Sv hybrid); DNA from clones was digested with *Nsi*1 subjected to Southern blot procedure using a radioactive probe located outside of the 5′ arm. Eight of 82 clones analyzed were correctly targeted, but only one retained the 5′ loxP site. That clone was injected into blastocysts that were then transplanted into foster mothers. Chimeric pups that were positive for the transgene were bred with Rosa26-FLPer to remove the SV-Neo gene and then with C57BL/6 mice to remove Rosa26-FLPer. Genotyping was performed using a pair of primers that flank the 5′ loxP site.

Virus Production
pAAV-hSyn-DIO-hM3Dq:mCherry, pAAV-Ef1α-DIO-mCherry, and pAAV-hSyn-dF-HA-KORD:mCitrine DNA plasmids were provided by B. Roth (Addgene, plasmids #44361, #50462, #65417). pAAV-Ef1α-DIO-ChR2:YFP and pAAV-hSyn-DIO-YFP DNA plasmids were provided by K. Deisseroth (Stanford University). pAAV-Ef1α-DIO-synaptophysin:mCherry DNA plasmid was generated from pAAV-Ef1α-DIO-synaptophysin:GFP by replacing the GFP fragment with mCherry (Roman et al., 2016). pAAV-CBA-FLP:DsRed and pAAV-CBA-DIO-GCamp6m DNA plasmids were provided by L. Zweifel. pAAV-CBA-DIO-GFP:TeTx was constructed by R. Palmiter (Han et al., 2015). Viruses were prepared in-house by transfecting HEK cells with each of these plasmids plus pDG1 (AAV1 coat stereotype)

helper plasmid; viruses were purified by sucrose and CsCl gradient centrifugation steps, and re-suspended in 0.1 M phosphate-buffered saline (PBS) at about 10^{13} viral particles/mL.

Stereotaxic Surgery
Mice were anesthetized with isoflurane and placed on a robotic stereotaxic frame (Neurostar). Virus was injected unilaterally or bilaterally as described in the text in the PBN (antero-posterior (AP) −5.00 mm; medio-lateral (ML) +/−1.35 mm; dorso-ventral (DV) 3.40) at a rate of 0.2 μl/min for 2.5 min. In mice used for optogenetic experiments, two custom-made fiber optic cannulas were implanted bilaterally above the PBN (AP −5.00 mm, ML ± 1.75 mm, DV 3.0), CeA (AP, −1.20 mm, ML ± 2.9 mm, DV 4.50 mm), BNST (AP 0.14 mm, ML ± 1.20 mm, DV 4.00 mm), or VPMpc (AP −1.80 mm, ML ± 1.25 mm, DV 3.00 mm) and affixed to the skull with C&B Metabond (Parkell) and dental acrylic. Mice were allowed to recover for 3 to 5 week before start of behavioral tests.

Photostimulation
After recovery from surgery, mice were acclimated to dummy cables attached to the implanted fiber optic cannulas. For CTA and food-intake studies, bilateral branching fiber optic cables (200-μm diameter, Doric Lenses) were attached to the head of each mouse before presentation of sucrose or food. Light-pulse trains (10 ms; 3 s on, 2 s off) were delivered at 5 Hz or 30 Hz for 5, 30, or 120 min as described in the text. Stimulation paradigms were programmed using a Master8 (AMPI) pulse stimulator that controlled a blue-light laser (473 nm; LaserGlow). The power of light exiting each side of the branching fiber optic cable was adjusted to 10 ± 1 mW.

Conditioned Taste Aversion (CTA) Assay
Mice were individually housed in custom cages with angled ports for placement of 2 test tubes of water. After 7 d of acclimation to the cage and bottles, mice were water deprived overnight. On days 1-3, mice had access to water for 30 min approximately 4 h after the onset of the light cycle and for 1 h before the onset of the dark cycle. On day 4, mice were given 30 min access to a novel 5% sucrose solution, followed by an injection of LiCl, LPS, CNO, or photostimulation. Water was available for 1 h in the afternoon and again on day 5, following the same schedule as days 1-3. This conditioning was repeated on days 6 and 7. On day 8, mice were given access to two bottles (water and 5% sucrose) for 30 min. The volume consumed was recorded in grams and converted to milliliters.

For calcium imaging and tetanus toxin (TeTx) experiments, *ad libitum*-fed mice were presented with a test tube of vanilla-flavored Ensure approximately 2 h after the onset of the light cycle. Twenty min after the first lick, mice were injected with LPS (50 μg/kg) and the Ensure bottle was removed after 4 h. Activity of CGRP^{PBN} neurons was measured on re-exposure to Ensure 2 d after conditioning. Surgery on mice for TeTx experiments was performed 3 or 4 d after conditioning and mice were allowed to recover for 3 weeks before testing for CTA.

Measuring Food Intake
After CTA, mice were allowed to recover for 7 d with *ad libitum* access to food and water. During this time, mice were also acclimated to a different rodent diet (D12450B, Research Diets), which was less susceptible to crumbling during consumption.

For manipulations of CGRP^{PBN} neurons with CNO and SalB, mice were acclimated to BIODAQ recording chambers (Research Diets) for 7 d. Food was removed 5 h prior to the start of the dark cycle each day and returned 15 min after lights out. Baseline food intake was measured for 3 d after the acclimation period and averaged. The next day, mice were given an injection of CNO 15 min prior to the start of the dark cycle and an injection of SalB at lights out. Food was returned 15 min into the dark cycle and consumption was measured overnight.

For photostimulation of CGRP^{PBN} axons, mice were fasted overnight then food restricted to 90% of their pre-fasting body weight for 3-4 d. During baseline food-intake measurements, optic fibers were bilaterally connected to the fiber optic cannulas on the head of mice but no laser stimulation was given. Mice were given access to food for 2 h and the amount consumed was recorded. The next day, mice were photostimulated for 30 min at 30 Hz and food consumed over 2 h was recorded.

Calcium Imaging
Mice were prepared for calcium imaging as described (Resendez et al., 2016). Briefly, 3 weeks after AAV-CBA-DIO-GCaMP6m viral injection, mice were anesthetized with isoflurane and implanted with a microendoscope lens (6.1 mm length, 0.5 mm diameter; Inscopix #100-000588) with assistance of a ProView implant kit (Inscopix, #100-000754) that allowed visualization of fluorescent activity during implantation. The lens was targeted to be ∼200–300 μm above the neurons using the following coordinates: AP −4.80 mm, ML −1.70 mm, DV 3.20 mm. One week after lens implantation, mice were anesthetized and a baseplate (Inscopix, #100-000279) was implanted above the lens. The baseplate provides an interface for attaching the miniature microscope during calcium imaging experiments, but at other times a baseplate cover (Inscopix, #100-000241) was attached to prevent damage to the microendoscope lens. Calcium fluorescence was recorded with nVista acquisition software (Inscopix) at 5 frames/s. Ethovision XT10 (Noldus Technology) was used to synchronize calcium recordings with behavioral video recordings. The recording parameters were based on pilot studies that demonstrated the least amount of photobleaching while allowing sufficient detection of fluorescent activity. Videos were processed with Mosaic software (Inscopix). Constrained non-negative matrix factorization for microendoscope data (CNMF-E) analysis was used to correct for neuropil contamination and background fluctuations in fluorescence caused by movement (Zhou et al., 2018). All detected calcium transients were visibly inspected for each cell to verify accuracy.

Raster plots show $dF/F = [(F-F_{baseline})/F_{max}] * avg(F_{max}-F_{min})$. $F_{baseline}$ is the average fluorescence during the 10 s before Ensure, F_{max} is the maximum fluorescence for the entire analyzed period (including 10 s baseline and 40 s post Ensure), and $avg(F_{max}-F_{min})$ is the average difference between F_{max} and F_{min} of each cell in an individual animal. This calculation placed the data from all the animals onto the same scale for comparison purposes. Distance traveled was analyzed with nose-point detection in Ethovision to track head movements during calcium imaging recordings. Pearson correlations between fluorescence change and head movement for each neuron was calculated and plotted as an r value, where 0 equals no correlation.

For average changes in fluorescence (Figures 3D and 3F), $dF/F = F-F_{baseline}/F_{baseline}$ where $F_{baseline}$ is the average fluorescence 30 s immediately prior to Ensure presentation and F is the average of each cell during 90 s after Ensure. Velocity was analyzed with mouse center-point detection in Ethovision during the 90 s post-Ensure period.

Slice Electrophysiology

Mice were deeply anesthetized with isoflurane and intracardially perfused with 10 mL of cold (4-6°C) cutting solution containing (in mM): 92 N-methyl-D-glucamine, 2.5 KCl, 1.25 NaH$_2$PO$_4$, 30 NaHCO$_3$, 20 HEPES, 25 D-glucose, 2 thiourea, 5 Na-ascorbate, 3 Na-pyruvate, 0.5 CaCl$_2$, 10 MgSO$_4$. Coronal slices (200 μm) were prepared using a vibrating microtome (VT1000S, Leica Biosystems) then allowed to recover for 10 min at 32°C in the same cutting solution. Slices were then transferred to a room temperature recovery solution containing (in mM): 92 NaCl, 2.5 KCl, 1.25 NaH$_2$PO$_4$, 30 NaHCO$_3$, 20 HEPES, 25 D-glucose, 2 thiourea, 5 Na-ascorbate, 3 Na-pyruvate, 2 CaCl$_2$, 2 MgSO$_4$ and allowed to equilibrate for an additional 45 min. Recordings were made in artificial cerebral spinal fluid containing (in mM): 126 NaCl, 2.5 KCl, 1.2 NaH$_2$PO$_4$, 18 NaHCO$_3$, 11 D-glucose, 2.4 CaCl$_2$, 1.2 MgCl$_2$ continuously perfused at a rate of ~2 ml/min at 32°C. All solutions were continuously oxygenated with 95% O$_2$-5% CO$_2$ (pH 7.3-7.4, 300-310 mOsm). Whole cell patch-clamp recordings were obtained using a MultiClamp 700B amplifier (Molecular Devices) and filtered at 1 kHz. Only data from cells with series resistance values < 25 MΩ which did not vary >20% during the experiment were included in data analysis.

For spontaneous EPSCs and AMPA/NMDA currents, bicuculline (10 μM) was included in the bath and patch electrodes (3-5 MΩ) were filled with an internal solution containing and (in mM): 120 CsMeSO$_3$, 20 HEPES, 0.4 EGTA, 2.8 NaCl, 2.5 Mg-ATP, 0.25 Na-GTP, 5 QX-314 bromide, pH 7.3, 290 mOsm. Electrodes also contained 0.2% biocytin to label recorded cells. CGRP neurons, as identified by GFP or mCherry epifluorescence, were held at $V_{hold} = -70$ mV and spontaneous EPSCs were recorded for 1 min. A concentric bipolar electrode placed in the superior cerebellar peduncle delivered 1-ms stimuli at 0.1 Hz to elicit AMAPR-mediated currents. 15 traces were average per cell then V_{hold} was stepped to +40 mV. NMDAR-mediated currents were measured as the average EPSC amplitude between 11 and 15 ms following the stimulus artifact, after the AMPA component had largely decayed. After the experiment, slices were fixed in 4% paraformaldehyde (PFA) overnight then cryoprotected in 30% sucrose and frozen for histology.

For recording of action potentials following current injection, patch pipettes were filled with an internal solution containing (in mM): 130 K-gluconate, 10 HEPES, 5 NaCl, 1 EGTA, 5 Mg-ATP, 0.5 Na-GTP, pH 7.3, 290 mOsm.

Evoked AMPA/NMDA currents and action potentials were analyzed offline using Clampfit 10.3 (Axon Instruments) software. Spontaneous EPSCs were analyzed with an automated detection protocol in MiniAnalysis (Synaptosoft) and manually checked for accuracy.

Pharmacological Injections

All pharmacological agents, with the exception of SalB, were prepared in sterile water and administered intraperitoneally (i.p.). These include: LiCl (0.2 M at 15 ml/kg; Fisher #L121), LPS, *S. typhimurium* (50 μg/kg; Calbiochem, #437650), and CNO (1 mg/kg; RTI #C929). SalB (10 mg/kg; Cayman Chemical #11488) was dissolved in DMSO and injected subcutaneously as described (Vardy et al., 2015).

Histology and Microscopy

Mice were anesthetized with Beuthansia (0.2 ml, i.p.; Merck) and perfused transcardially with PBS followed by 4% PFA in PBS. Brains were post-fixed overnight in 4% PFA at 4°C, cryoprotected in 30% sucrose, frozen in OCT compound (ThermoFisher), and stored at −80°C. Coronal sections (30 μm) were cut on a cryostat (Leica Microsystems) and collected in cold PBS. For Fos studies, mice were photostimulated for 15 min or given CNO and/or SalB 90 min before perfusion.

For immunohistochemistry experiments, sections were washed three times in PBS with 0.2% Triton X-100 (PBST) for 5 min and incubated in blocking solution (3% normal donkey serum in PBST) for 1 h at room temperature. Sections were incubated overnight at 4°C in PBST with primary antibodies including: rabbit anti-c-Fos (1:2000, Abcam, ab190289), goat anti-c-Fos (1:500, Santa Cruz Biotechnology, sc-52), chicken-anti-GFP (1:10000, Abcam, ab13970), and/or mouse-anti-CGRP (1:1000, Abcam, ab 81887). Slices from electrophysiology experiments were incubated in streptavidin conjugated to marina blue (1:2000, ThermoFisher, S11221). After 3 washes in PBS, sections were incubated for 1 h in PBS with secondary antibodies: Alexa Fluor 488 donkey anti-chicken, Alexa Fluor 594 donkey anti-mouse, Cy5 donkey anti-goat, and/or Cy5 donkey anti-rabbit (1:500, Jackson ImmunoResearch). Tissue was washed 3 times in PBS, mounted onto glass slides, and coverslipped with Fluoromount-G (Southern Biotech).

Fluorescent images were acquired using a Keyence BZ-X700 microscope. Images were minimally processed using ImageJ software (NIH) to enhance brightness and contrast for optimal representation of the data. All digital images were processed in the same way between experimental conditions to avoid artificial manipulation between different datasets.

QUANTIFICATION AND STATISTICAL ANALYSIS

An online power and sample size calculator was used to determine an effective sample size for statistical comparisons (http://powerandsamplesize.com). Based on a pilot study for CTA, we used a mean sucrose preference of 0.4 and s.d. of 0.2. Assuming a significance level of 0.05 and power of 0.8, we calculated a sample size of 4 mice per group if means were 2-fold different with a two-tailed Student's t test. SigmaPlot 12.0 (Systat Software) was used for all other statistical analysis. For all data, normality was tested using the Shapiro-Wilk test to determine whether parametric or non-parametric analyses were required. The asterisks in the figures represent the p values of post hoc tests corresponding to the following values $*p < 0.05$, $**p < 0.01$, $***p < 0.001$. Data and figures were exported into CorelDraw X6 (Corel) for preparation of figures.

Following histology and imaging, any mouse whose targeted injection site was missed or demonstrated very sparse expression ($\leq$10 fluorescent neurons/section at bregma -5.1) was excluded from experimental analysis.